EVAPOTRANSPIRATION MAPPING WITH METRIC TO EVALUATE EFFECTIVENESS OF IRRIGATION IN FLOOD MITIGATION FOR THE DEVILS LAKE BASIN

H. Büyükcangaz, D. D. Steele, S. R. Tuscherer, D. G. Hopkins, X. Jia

ABSTRACT. *A period of excess precipitation since 1993 in the Devils Lake basin in northeastern North Dakota has caused extensive flooding of agricultural land and has raised the question of whether irrigation of agricultural crops to increase evapotranspiration (ET) might be an effective way to remove water from the basin. The objectives of this study were to compare ET estimates derived from application of the Mapping ET at High Resolution with Internalized Calibration (METRIC) algorithm for North Dakota conditions ($METRIC_{ND}$) under irrigated and rainfed conditions and to assess the potential for irrigation to increase crop ET as a flood mitigation strategy. Weather data, land use maps, and Landsat 5 Thematic Mapper imagery from 2006, 2007, and 2008 were used as inputs to the $METRIC_{ND}$ model. The ET for irrigated crops ($ET_{Irrigated}$) was estimated at five test sites from the Devils Lake Basin Water Utilization Test Project (DLBWUTP). The ET for the predominantly rainfed study area ($ET_{Rainfed}$) was estimated using land use maps to identify locations of the same crops as were present on the test sites. The $METRIC_{ND}$ model was compared to ET values derived from an eddy covariance (EC) system for approximately two months in 2007 at an irrigated alfalfa test site in the DLBWUTP; the mean absolute error between $METRIC_{ND}$ and the EC system for the comparison period was 0.51 mm d^{-1}. Linear regression of ET (in mm) for the test sites and the larger study area yielded $ET_{Irrigated} = 1.23 \times ET_{Rainfed} + 4.77$ with $R^2 = 0.96$, and a t-statistic indicated that the slope was greater than 0 at $p = 0.001$, indicating the potential for increased ET under irrigation. However, addition of large volumes of irrigation water to the predominantly poorly drained soils in the basin will cause waterlogging and trafficability problems. Installation of subsurface drainage may help alleviate waterlogging, improve crop productivity, and increase ET, but subsurface drainage brings its own complications of disposal of the drained water, salinity of the drainage effluent, and possible sodicity problems on some soils.*

Keywords. *Drainage, Evapotranspiration mapping, Irrigation, METRIC, Landsat 5, Remote sensing, Satellite imagery, SEBAL.*

The Devils Lake basin in northeastern North Dakota is a 0.99 Mha area with no outflow in recent history. Excessive precipitation since 1993 caused the water level in Devils Lake to rise 9.0 m from 1993 to 2010 (NDSWC, 2010). This increase in the lake's water level has caused flood damage and loss of land, roads, and other resources. One of the solutions proposed to lessen the damage and control flooding included the use of upper basin water for irrigation of agricultural crops. The difference in evapotranspiration (ET) between irrigated and rainfed crops would be assumed to represent the capabilities of irrigation to remove water from the Devils Lake basin.

The Devils Lake Basin Joint Water Resource Board (DLBJWRB) initiated the Devils Lake Basin Water Utilization Test Project (DLBWUTP) in the upper basin of Devils Lake involving irrigation on about eight quarter sections (65 ha parcels) of land. One objective of the test project was to assess whether full irrigation, augmented by a "water wasting" addition, could use excess water in the basin for flood mitigation. This objective was developed as a result of a reconnaissance-level survey conducted by Bartlett and West Engineers, Inc., of Bismarck, North Dakota (Bartlett and West, 2002). Thirty-five applicants volunteered land for this test. Benefits to the producers included anticipated revenues from irrigation and a chance to purchase irrigation equipment at reduced cost following the test project. If the test phase of the project was considered successful, a pilot phase was planned that would have developed irrigation on about 1600 ha. If the pilot phase was successful, full implementation amounting to irrigation on about 8100 ha would have been initiated.

Instrumentation for point-based measurements of ET at many sampling locations would be cost-prohibitive in the Devils Lake basin situation. Therefore, it would be advantageous to use remote sensing based techniques to estimate ET over large areas to compare irrigated and rainfed fields in the basin. Procedures for ET estimation on large spatial scales have been developed using a remote sensing approach cou-

Submitted for review in October 2016 as manuscript number NRES 12149; approved for publication by the Natural Resources & Environmental Systems Community of ASABE in June 2017.

The authors are **Hakan Büyükcangaz,** Associate Professor, Department of Biosystems Engineering, Uludag University, Bursa, Turkey; **Dean D. Steele, ASABE Member,** Associate Professor, Department of Agricultural and Biosystems Engineering, **Sheldon R. Tuscherer,** Research Specialist, Department of Agricultural and Biosystems Engineering, **David G. Hopkins,** Associate Professor, Department of Soil Science, and **Xinhua Jia, ASABE Member,** Associate Professor, Department of Agricultural and Biosystems Engineering, North Dakota State University, Fargo, North Dakota. **Corresponding author:** Dean Steele, Dept. 7620, P.O. Box 6050, North Dakota State University, Fargo, ND 58108-6050, phone: 701-231-7268; e-mail: Dean.Steele@ndsu.edu.

  ISSN 2151-0032 https://doi.org/10.13031/trans.12149

pled with ground-based weather data to estimate the components of the surface energy balance given by:

$$LE = R_n - G - H \quad (1)$$

where LE is the latent energy of vaporization, which is computed as the residual of net radiation (R_n), soil heat flux (G), and sensible heat flux to the atmosphere (H), with all terms expressed in W m^{-2} and typically integrated over hourly or daily time steps. Latent energy is equivalent to the energy used for ET. Bastiaanssen et al. (1998a, 1998b) implemented this approach in their Surface Energy Balance Algorithm for Land (SEBAL). The SEBAL model was modified by Allen et al. (2007a, 2007b) and denoted Mapping ET at High Resolution with Internalized Calibration (METRIC). Allen et al. (2007a) described modifications in the METRIC model compared with the SEBAL model. METRIC uses a well-watered, full-cover crop (Allen et al., 2007a) rather than a water surface for the "cold" pixel. A daily soil water balance model is used in METRIC to accommodate nonzero evaporation, rather than SEBAL's approach of assuming LE = 0 at the "hot" or dry pixel. The METRIC algorithms scale up instantaneous ET to daily ET by assuming that the instantaneous crop coefficient (K_c) is valid throughout the day of the satellite image, whereas SEBAL extrapolates instantaneous ET to daily ET by assuming a constant value of the evaporative fraction (Bastiaanssen et al. 1998b, 2005), with the latter defined as LE/(R_n + G).

Applications of SEBAL and METRIC have been made in a variety of settings worldwide (Allen et al., 2007b; Bastiaanssen et al., 1998b; Singh et al., 2008; Chavez et al., 2012). In an early application of METRIC, Allen et al. (2007b) found that four monthly ET estimates agreed within ±16% of lysimeter measurements of ET at Montpelier, Idaho, and that when summed over the four-month period, the agreement was within 4%. Compared to sugar beets on weighing lysimeters at Kimberly, Idaho, Allen et al. (2007b) found that ET_{METRIC} agreed within an average of 14% for seven image dates in 1989, and the seasonal ET totals agreed within 1%. Singh et al. (2008) compared SEBAL ET (ET_{SEBAL}) estimates with Bowen ratio energy balance system (BREBS) measurements of ET (ET_{BREBS}) in south-central Nebraska and found a root mean square difference of 1.04 mm d^{-1} for seven image dates in 2005. Their results were also reported as $ET_{SEBAL} = 0.948 \times ET_{BREBS}$. On a seasonal basis, their ET_{SEBAL} estimates were within 5% of the ET_{BREBS} measurements. Chavez et al. (2012) compared ET_{METRIC} estimates based on airborne remotely sensed images with hourly and daily ET measurements from large weighing lysimeters (ET_{LYS}) at Bushland, Texas, for six image dates in 2007. Their imaging system had a pixel resolution of 0.5 m for the visible and near-infrared bands and 1.8 m for the thermal infrared band, compared with 30 to 120 m pixel resolutions for Landsat 5 or 7 imagery. For all the data sets considered, they obtained mean bias errors (MBE, where MBE = $ET_{METRIC} - ET_{LYS}$) of -0.06 mm h^{-1} and -0.15 mm d^{-1} and root mean square errors of 0.19 mm h^{-1} and 1.91 mm d^{-1}. When expressed as a percentage of alfalfa reference ET, the hourly and daily MBE values were -6.32% and -1.2% and the RMSE values were 23.58% and 19.63%, respectively.

In the literature, ET_{METRIC} estimates are typically divided by reference crop ET (ET_r) from weather station data to obtain estimates of the fraction of reference ET (ET_rF; Allen, 2007a), equivalent to the commonly used K_c. Morton et al. (2013) developed an automated METRIC calibration procedure that examined histograms of ET_rF for each simulation (i.e., image date and paired selection of hot and cold pixels), particularly the tails of the ET_rF distributions defined as the "hot pixel tail" with $ET_rF < 0.1$ and the "cold pixel tail" with $ET_rF > 1.05$. These limits on the ET_rF values constrain the model to represent realistic ET_rF values (Allen et al., 2011) and were the "primary measure for adjusting the calibration" of Morton et al. (2013). If the ET_rF histogram tails were too large, then recalibration was indicated, i.e., new hot and/or cold pixels were selected, and a new simulation was run. In their study, approximately 80% of the calibration simulations resulted in 0% to 8% of the pixel population in the hot pixel tail ($ET_rF < 0.1$) and 0% to 2% of the pixel population in the cold pixel tail ($ET_rF > 1.05$). Morton et al. (2013) compared their ET_{METRIC} estimates with ET_{BREBS} and eddy covariance (EC) measurements of ET (ET_{EC}) in Nevada for 16 monitoring periods ranging from 78 to 214 days. The averages of seasonal total measured ET and ET_{METRIC} were 692 and 712 mm, respectively, and the corresponding averages of daily ET were 4.24 and 4.39 mm.

Most or all ET mapping studies have been conducted in the context of water conservation; we are not aware of studies using ET mapping to assess the potential of irrigation to mitigate flooding. Intermittent flood waters are often captured in spate irrigation (UNW-AIS, 2013) or water banking systems (SRP, 2017), but these are solutions to take advantage of seasonal, short-term phenomena rather than mitigation of multi-year-duration flooding.

Although Steele et al. (2015) used SEBAL for ET mapping in the DLBWUTP, the SEBAL modeling was subcontracted to Davids Engineering, Inc., in Davis, California, as a one-time modeling effort. In addition to the SEBAL results, North Dakota State Water Commission personnel expressed interest in developing ET mapping capabilities that they could apply to other projects in the state. It was determined that use of the METRIC model and the already-available DLBWUTP data sets would be appropriate to initiate this effort. The objectives of this article are to (1) apply the METRIC algorithms (adapted to North Dakota) to compare ET for irrigated versus rainfed crops in the Devils Lake basin, and (2) assess the potential for irrigation of agricultural crops to increase ET and thereby remove water from the basin as a flood mitigation strategy.

Materials and Methods

Study Area and Instrumentation

Field data for this study were obtained for the 2006 through 2008 growing seasons in the DLBWUTP. Ten field sites (designated as "test sites" and numbered) were selected in the Devils Lake basin of northeastern North Dakota (fig. 1). The sites were equipped with center-pivot sprinkler

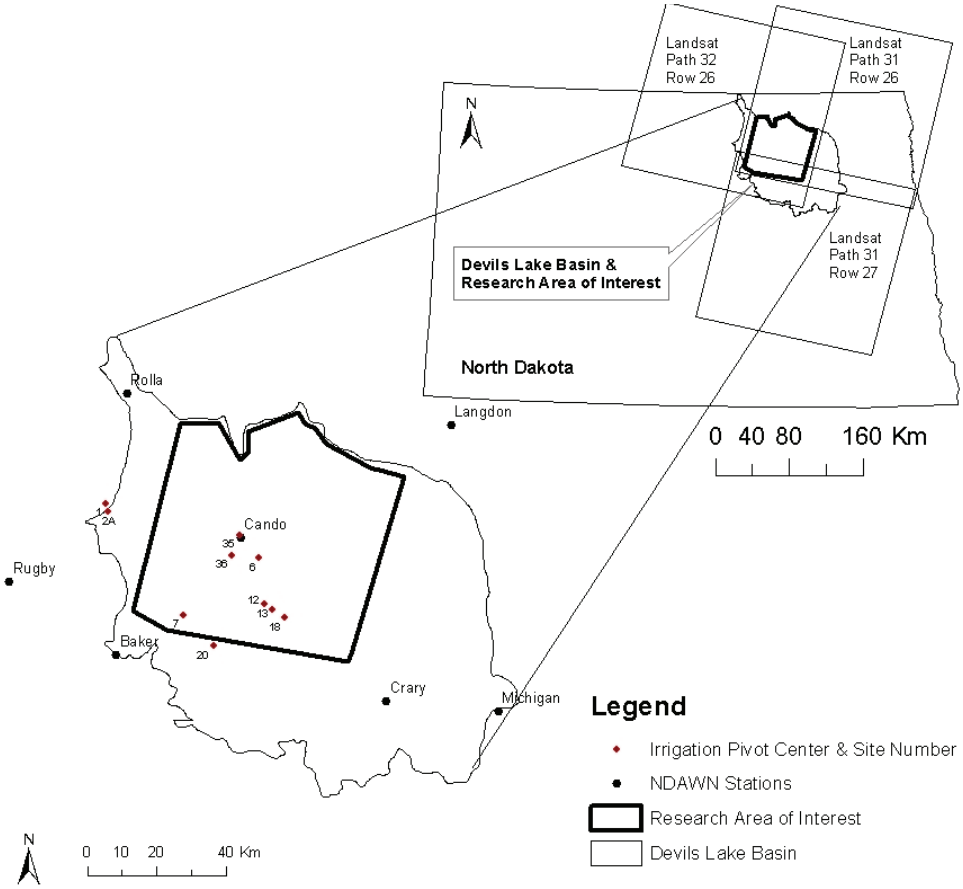

Figure 1. Devils Lake basin study area in North Dakota.

irrigation systems to enable comparisons of ET under irrigated and rainfed conditions in the predominantly rainfed basin (Steele and Hopkins, 2010; Steele et al., 2015). The sites were selected for participation in the study by the DLBJWRB in consultation with a consulting firm. Site selection was based on farmer or landowner participation, the presence of soil map units representative of the soils in the basin, proximity to surface water for irrigation, and suitability of irrigation water quality. The sites ranged in size from 5 to 49 ha. Twenty-five field monitoring stations were installed across the ten field sites. At each monitoring station, a 203 mm diameter tipping-bucket rain gauge (model 3554, Spectrum Technologies, Plainfield, Ill.) and a 100 mm diameter totalizing (manual) rain gauge (Stratus model, Productive Alternative, Inc., Fergus Falls, Minn.) were used to monitor amounts and dates of rainfall and irrigation. Additional measurements included soil moisture, deep percolation via fluxmeters, and groundwater depths via observation wells at selected locations (Steele and Hopkins, 2010). At site 20, soil water tension was measured with tensiometers (model "R," Irrometer Co., Inc., Riverside, Cal.) at 30 cm depths at stations A1, A3, and A4 at the site to indicate the degree to which the alfalfa was well-watered.

Table 1 describes the locations, soil types, irrigation status, field sizes, presence or absence of groundwater monitoring wells, and proximity of the groundwater to the surface water for each monitoring station. While sites 1 and 2A were part of the test project (Steele and Hopkins, 2010), they were omitted from the ET mapping area of interest because they were outside the overlap area of Landsat 5 paths 31 and 32. By constraining the study area to the image overlap area, temporal resolution is improved. A trade-off is recognized with a higher temporal frequency within the overlap area versus the additional area (at lower temporal resolution), which would have been available if both of the single-path regions were modeled separately.

Weather data were obtained from the Cando, North Dakota, station of the North Dakota Agricultural Weather Network (NDAWN, 2011). The Cando station (48.471° N, 99.166° W, 452.5 m elevation) was taken as the reference due to its central location within the image area of interest (AOI; fig. 1). Monthly ET and precipitation data for the study period are summarized in table 2. The NDAWN system is part of the High Plains Regional Climate Center (HPRCC) at the University of Nebraska-Lincoln. Daily and hourly data from stations in NDAWN are subjected to quality assurance and quality control (QA/QC) procedures conducted by the HPRCC. Data are checked against upper and lower limits, thresholds, and no-change-vs.-time rules for each variable (Hubbard, 2001; Meek and Hatfield, 2001). For example, solar radiation (R_s) measurements are checked against sunrise and sunset times to ensure physically realistic data and against clear-sky radiation (R_{so}) values to ensure $R_s \leq R_{so}$. Data are screened using measurements from surrounding stations; an exception is precipitation because of its high spatial variability. The NDAWN data are subjected to statis-

Table 1. Site and stations, locations, irrigation status, field sizes, and water table depths for the Devils Lake basin water utilization test project.

Site[a]	Station	Latitude (°N)	Longitude (°W)	SSURGO Soil Series	Irrigation Status	Center-Pivot System Radius (m)	Irrigated Area at Site (ha)	Water Table within 1.22 m of Soil Surface[b] 2006	2007	2008
6	A1	48.41792	99.09536	Hamerly-Barnes (F107A)	Irrigated	383	46.1	Yes	Yes	Yes
6	A2	48.41850	99.09951	Barnes-Buse (F144B)	Irrigated	-	-	No	No	No
7	A1	48.27116	99.39374	Balaton-Wyard (F167B)	Irrigated	395	49.0	No	Yes	No
7	A2	48.27129	99.39017	Hamerly-Tonka (F100A) and Balaton-Wyard (F167B)	Irrigated	-	-	-	-	-
7	A3	48.27127	99.38468	Barnes-Buse-Langhei (F143C)	Irrigated	-	-	-	-	-
7	A4	48.27563	99.38836	Hamerly-Wyard (F101A)	Rainfed	-	-	No	No	No
12	A1	48.29930	99.07640	Hamerly-Wyard (F101A)	Irrigated	395	49.0	Yes	Yes	Yes
13	A1	48.28496	99.04588	Vallers (F6A)	Irrigated	395	49.0	Yes	Yes	Yes
18	A1	48.26193	98.99593	Hamerly-Cresbard (F135A)	Irrigated	349	38.3	No	Yes	Yes
18	A2	48.26685	98.99954	Hamerly-Cresbard (F135A)	Rainfed	-	-	-	-	-
20	A1	48.19245	99.27122	Balaton-Wyard (F167B)	Irrigated	365	41.9	No	No	No
20	A3	48.19279	99.27182	Balaton-Wyard (F167B)	Irrigated	-	-	-	-	-
20	A4	48.19488	99.27415	Balaton-Wyard (F167B)	Mixed[c]	-	-	No	No	No
35	A1	48.47775	99.16956	Swenoda (F776B)	Rainfed	152	7.3	Yes	Yes	No
35	A2	48.47859	99.17273	Bearden (F431A)	Irrigated	-	-	Yes	No	No
36	A1	48.42503	99.19904	Bearden (F431A)	Irrigated	184	5.3	No	No	No
36	A2	48.42261	99.19920	Maddock-Hecla (F384B)	Rainfed	-	-	Yes	No	No

[a] Site numbers are not consecutive because sites were selected from approximately 40 fields in the initial applicant pool, and site identifiers were held constant thereafter. Additional sites outside the ET modeling area of this study are not included in the table. Site 36 was only a semi-circle.

[b] Dashes indicate that no observation well was present at the station.

[c] Site 20, station A4 was rainfed in 2006 and 2007 and irrigated in 2008.

Table 2. Monthly totals of daily ET and rainfall for May through September for 2006 through 2008. Data were taken from the Cando, North Dakota, station of the North Dakota Agricultural Weather Network.

	2006			2007			2008			1995-2016 Average		
Month	Penman ET (mm)	Rainfall (mm)	Diff. (mm)	Penman ET (mm)	Rainfall (mm)	Diff. (mm)	Penman ET (mm)	Rainfall (mm)	Diff. (mm)	Penman ET (mm)	Rainfall (mm)	Diff. (mm)
May	170	47	123	169	159	10	196	16	180	174	65	109
June	195	36	159	181	69	112	182	96	86	179	81	98
July	228	18	210	200	114	86	188	31	157	181	84	97
August	173	69	104	147	17	130	163	74	89	163	57	106
September	123	24	99	136	11	125	97	74	23	124	43	81
Total	889	194	695	833	370	463	826	291	535	821	330	491

tical techniques for outlier detection and estimation of missing values (K. Hubbard, HPRCC, Lincoln, Neb., 2014 personal correspondence) as part of the HPRCC's QA/QC procedures. When data are not available, estimates are computed by inverse distance weighting from the closest surrounding stations or by other procedures for estimation described by Hubbard (2001). Additional details on station siting, sensor maintenance, and data quality control procedures used by the NDAWN staff are available at the NDAWN website (NDAWN, 2011). In addition to the NDAWN QA/QC process, the procedures in the main body and in Appendix D of ASCE-EWRI (2005) were used to assess the integrity of the solar radiation, relative humidity (or dew point temperature), wind speed, and air temperature data from NDAWN. Daily data for April through October for each year of interest and hourly data for the dates of satellite images were assessed. Irrigation scheduling details were described by Steele et al. (2015). Crop types were recorded by research personnel, and emergence dates were based on observations by the farmer or operator at each field site.

METRIC APPLICATION

The METRIC model (Allen et al., 2005, 2007a, 2007b, 2012, 2013; Morton et al. 2013) was applied to the DLBWUTP area shown in figure 1. Allen et al. (2007a, 2007b) presented a detailed description of the METRIC model. Because the METRIC literature sometimes presents more than one mathematical formulation for the processes and relationships modeled, we present in this section the selections or alterations made in our application of the model (designated $METRIC_{ND}$). For example, Allen et al. (2005) presented two formulations for G/R_n, and here we specify which equation was used. Similarly, an alternative formulation of crop height (h) versus leaf area index (LAI) was used (discussed below). The remaining equations used for the $METRIC_{ND}$ modeling follow the METRIC literature cited above and are not repeated herein. Most of the image processing components of the $METRIC_{ND}$ algorithms were coded in the Spatial Modeler Language (SML) of ERDAS Imagine (ERDAS, 2010). Minor pre- and post-processing and modeling operations were performed using SML, the Model Maker of ERDAS Imagine for graphical models, commands available in ERDAS Imagine, and/or supporting spreadsheets.

Landsat 5 TM satellite images from Path 31 Row 26 (designated P31R26) and from P32R26 were obtained from the U.S. Geological Survey (USGS, 2011) for the 2006 through 2008 growing seasons (table 3). An AOI was defined in ERDAS Imagine to encompass as many field sites as possible while avoiding edges where pixels from one or more bands of the images were not present. The digital numbers of the images were converted to radiance and then to reflectance

Table 3. Landsat 5 TM images used in simulations.

No.	Date[a]	Day of Year	Days in Interval[b]	Path	Row
1	20 May 2006	140	40	31	26
2	28 June 2006	179	10	32	26
3	7 July 2006	188	8	31	26
4	14 July 2006	195	10	32	26
5	23 July 2006	204	8	31	26
6	30 July 2006	211	10	32	26
7	8 Aug. 2006	220	8	31	26
8	15 Aug. 2006	227	-	32	26
9	8 June 2007	159	8	31	26
10	15 June 2007	166	42	32	26
11	26 July 2007	207	8	31	26
12	2 Aug. 2007	214	10	32	26
13	11 Aug. 2007[c]	223	8	31	26
14	18 Aug. 2007	230	17	32	26
15	3 Sept. 2007	246	10	32	26
16	12 Sept. 2007	255	8	31	26
17	19 Sept. 2007	262	-	32	26
18	1 June 2008[d]	153	81	32	26
19	20 Aug. 2008	233	10	32	26
20	29 Aug. 2008	242	-	31	26

[a] The overpass time for all images was 17:00 GMT (11:00 a.m. Central Standard Time in the U.S.).

[b] The days in each interval include the starting and ending dates because one image layer is needed to represent ET_rF for each day. For example, 7 to 14 July 2006 is a seven-day interval, but eight ET_rF layers were developed, one for each day. Duplicate layers were omitted when compiling ET totals across multiple intervals.

[c] The 11 August 2007 scene was omitted from interpolation of ET_rF due to wet conditions and the unavailability of qualified cold pixels necessary to adjust the image so the ET_rF histogram fit within its upper and lower constraints. Interpolations were performed from 2 to 18 August.

[d] The 1 June 2008 scene was omitted from interpolation of ET_rF because of the uncertainty in crop development rates during the long time interval to the next usable image date on 20 August 2008.

using the metadata from each Landsat 5 image header file and the equations provided by Chander et al. (2009). Cloud-covered areas and cloud shadows on the ground surface were removed by manually inspecting at-surface reflectance images and manually creating masks using the ERDAS AOI tool wherever needed. The original images were subset to the AOIs, creating an image of clouds and cloud shadows. A graphical or SML model was then used to write values of 0 under clouds and values of 1 under non-cloud areas. Next, the model accepted original image values where cloud masks were not present and wrote 0 values under clouds and cloud shadows, thereby "cutting out" clouds and cloud shadows. Images with full or predominant cloud cover were not used.

The momentum roughness length (z_{om}) was calculated as:

$$z_{om} = 0.12h \tag{2}$$

where h is crop height (m). Allen et al. (2005) presented estimates of h as a function of LAI for alfalfa, corn, potato, beans, beets, peas, and spring and winter wheat. In this study, height versus LAI functions for all crops except corn were approximated by:

$$h = 0.15\text{LAI} \tag{3}$$

as noted by Allen et al. (2005). Because corn, a common crop in the Devils Lake basin, has a different plant architecture and height compared with other agricultural crops, the relationship:

$$h = 0.7\text{LAI}^{0.61} \tag{4}$$

developed by Anderson et al. (2004) was used to represent corn. The power function was preferred to a polynomial function because the latter could rise unrealistically at high values of LAI. A minimum z_{om} value of 0.005 m was assigned for barren soil.

Soil heat flux (G, W m^{-2}) was estimated using Bastiaanssen's (2000) equation:

$$\frac{G}{R_n} = T_s\left(0.0038 + 0.0074\alpha\right)\left(1 - 0.98\text{NDVI}^4\right) \tag{5}$$

where T_s is surface temperature (°C), α is surface albedo (dimensionless), and NDVI is normalized difference vegetation index (dimensionless).

Earth-sun distances were obtained from Chander et al. (2009). A "flat model" was used rather than a "mountain model" (Allen et al., 2005), i.e., no adjustments were made in the solar incidence angle. The Devils Lake basin is in the Great Plains region, and undulations in the local terrain were considered small enough to obviate the need to use the mountain model (confirmed by R. Allen, 2012 personal correspondence).

Incoming longwave radiation ($R_{L\downarrow}$, W m^{-2}) can be calculated for each pixel with the Stefan-Boltzmann equation:

$$R_{L\downarrow} = \varepsilon_a \sigma T_a^4 \tag{6}$$

where ε_a is the effective atmospheric emissivity (dimensionless), σ is the Stefan-Boltzmann constant (5.67×10^{-8} W m^{-2} K^{-4}), and T_a is the near-surface air temperature (K). Allen et al. (2007a) stated, "In most applications of METRIC, the surface temperature (T_s) of each image pixel has been used as a surrogate for T_a in [equation 6], which suggests that incoming long-wave radiation varies across an image in proportion to the underlying surface temperature." In this study, T_s was used in equation 6 on a pixel-by-pixel basis based on the modified Planck equation using procedures for the corrected thermal radiance as described by Allen et al. (2012).

The first SML module calculated R_n, T_s, G, NDVI, LAI, and related parameters. The values of air temperature, relative humidity, and elevation were taken from the Cando weather station in the NDAWN system (fig. 1). Classification of land use and crop type was based on estimates from a cropland data layer image (CDL; USDA-NASS, 2007, 2008, 2009) with spatial resolution of 54 m for each season. Hot and cold pixels were selected using criteria described by Allen et al. (2005, 2012). Starting with the T_s image, a modified image was developed (and denoted as a "cold pixel screening image") in which T_s pixel values were retained as viable cold pixel candidates defined by the criteria $0.18 \le \alpha \le 0.24$, $0.76 \le \text{NDVI} \le 0.84$, and $\text{LAI} \ge 3$, while T_s pixels were set to 0 elsewhere to eliminate them from further consideration. A color gradation of nonzero T_s values with black where $T_s = 0$ allowed quick identification of cold pixel candidates meeting the α, NDVI, and LAI criteria while simultaneously allowing cross-checking of surface temperatures. Similarly, a "hot pixel screening image" was developed based on the criteria $0.17 \le \alpha \le 0.23$, $0.10 \le \text{NDVI} \le 0.15$,

and 0.0 ≤ LAI ≤ 0.4 as viable hot pixel candidates. The NASS CDL, the at-surface reflectance images produced as an intermediate step in the $METRIC_{ND}$ process, and our field visits to and familiarity with the area were also used in the cold and hot pixel selection processes. The coldest and hottest pixels in the respective screening images (not the original images) were generally selected for cold and hot pixels, respectively. This is similar to the automated calibration process described by Allen et al. (2013), in which they selected the coldest 20% of the highest 5% of NDVI pixels and the hottest 20% of the lowest 10% of NDVI pixels.

The FAO-56 soil water balance model (Allen et al., 1998, 2012; Allen, 2011) was employed using daily rainfall from the Cando NDAWN station and SSURGO data (USDA-NRCS, 2011) for soil texture to account for nonzero evaporation ($ET_rF > 0$) at the hot pixel due to residual evaporation and recent rainfall. If no rain occurred on the image date, the FAO-56 procedure as described by Allen et al. (2012) was used. If rain occurred on the image date, hourly rainfall for that day was examined to see if the rain might have fallen after the image acquisition time and thus warranted a low ET_rF value at the hot pixel. For example, in 2006, the daily rainfall record indicated that no rain fell from 23 through 29 July and 12.4 mm of rain fell on 30 July, resulting in an FAO-56 prediction of $ET_rF = 0.846$ at a hot pixel location for 30 July. The Landsat 5 image metadata recorded a scene center scan time of 11:21:59 (Central Standard Time) on 30 July, whereas the hourly rainfall record for that day indicated that the rain occurred as 0.3, 4.0, and 8.1 mm for each of the hours ending at 21:00, 22:00, and 23:00, respectively. Therefore, the surface of the landscape was assumed to still be in the prior days' dry condition at the time of image acquisition. Based on these findings, the rainfall for 30 July was set to 0 in the daily time step FAO 56 model, which as a result predicted a 30 July value of $ET_rF = 0$ for use in the $METRIC_{ND}$ model at the hot pixel.

The second SML module calculated instantaneous *H*, LE, and daily ET. For the sensible heat algorithm, a spreadsheet (Allen et al., 2005) was used to calculate parameters *a* and *b* in:

$$dT = b + aT_s \tag{7}$$

where *dT* is the temperature difference (K) driving sensible heat at the soil surface, i.e.:

$$H = \frac{\rho c_p dT}{r_{ah}} \tag{8}$$

where ρ is air density (kg m^{-3}), c_p is the specific heat of air (1004 J kg^{-1} K^{-1}), and r_{ah} is the aerodynamic resistance to heat transfer (s m^{-1}).

Hourly and daily reference ET (ET_r) estimates were calculated according to the ASCE-EWRI standardized Penman-Monteith method (ASCE-EWRI, 2005) using Ref-ET software (Allen, 2002) with NDAWN weather station data (NDAWN, 2011).

The looping capabilities of SML were employed in the second SML module to apply the stability correction factors and solve the sensible heat flux component of the energy balance, as described by Allen et al. (2007a), for all pixels in an image or scene of interest. Allen et al. (2012) stated that four or five iterations are generally sufficient to obtain convergence of *H*. In this study, the use of ten iterations was hypothesized as sufficient to achieve convergence of *H* values to within 0.1% relative change for all pixels, and the convergence was tested as follows. Successive iterations of *H* estimates for all pixels in the study area were stacked as adjacent layers in an image, and the maximum relative change in *H* for iteration *i* was calculated as:

$$\Delta H_i\ (\%) = GlobalMax\left\{\left|\frac{H_i - H_{i-1}}{H_{i-1}}\right|\right\} \times 100 \tag{9}$$

where *GlobalMax* is the global maximum function in SML, H_i and H_{i-1} are the *i*th and (*i*−1)th iterations, respectively, of the sensible heat estimate at each pixel, and $i = 2, 3, ..., n$, where $n = 10$ is the maximum number of iterations used.

Spatial estimates of ET from $METRIC_{ND}$ were divided by ET_r calculated from data from the Cando NDAWN station to obtain spatial estimates of ET_rF. Pixel values of ET_rF less than 0, assumed caused by systematic and random errors propagated through the model (Allen et al., 2007a), were not set to 0, although we recognize that negative ET is not physically possible. Similarly, pixel values of ET_rF exceeding the 1.05 value used for the cold pixel were not set to 1.05 as an upper limit. Conditional statements in SML code were used to eliminate nonagricultural land classifications, such as water, wetlands, urban, developed, forest, trees, and shrubland, from the analyses because these land uses are beyond the scope of the agricultural basis of the $METRIC_{ND}$ algorithms employed herein. The remaining distributions of ET_rF for agricultural pixels were expected to lie within the range of $0 \le ET_rF \le 1.05$.

To assess model results and determine whether further calibrations (i.e., alternate hot and cold pixel selections) were necessary, histograms of ET_rF were examined for the simulations after eliminating nonagricultural land uses from consideration using the NASS CDL ground cover databases (USDA-NASS, 2007, 2008, and 2009). Following the constraints on ET_rF used by Morton et al. (2013), hot and cold pixel selections were adjusted to limit the populations of pixels to a maximum of 7.5% for pixels with $ET_rF < 0.1$ and a maximum of 2% for pixels with $ET_rF > 1.05$.

Because Landsat 5 has 120 m thermal pixels and 30 m visible and near-infrared pixel sizes, thermal pixels near field or crop boundaries may be contaminated by thermal processes outside a field or crop of interest (Allen et al., 2007b; Morton et al., 2013). Details on the need for and procedures to ensure homogeneity in thermal pixels were presented by Allen et al. (2013), who used the standard deviation (SD) of land use class numbers within a 7-pixel by 7-pixel cluster or window of pixels for each pixel in a Landsat 5 image. This is equivalent to application of the Focal Standard Deviation (FSD) function in ERDAS Imagine, with a 7 × 7 focal window, to land use classes in the National Land Cover Database (NLCD; USGS, 2012). With an SD of 0, each pixel of interest is centered within a 7 × 7 window of uniform land use. For 30 m × 30 m pixels sizes in Landsat 5, the buffering distance from the center to the edge of a 7 × 7

window is 3.5 pixels × 30 m pixel^{-1} = 105 m. A 105 m thermal buffering distance was also used by Clark et al. (2007) for Landsat 5 images under the assumptions that fields are generally rectangular in shape and that pixel and field boundaries are usually parallel, assumptions that are generally valid in North Dakota agricultural settings. To facilitate the use of SD to identify uniformly cropped areas, Allen et al. (2013) suggested recoding all agriculturally related land use classes in the NLCD to the same value.

In this study, thermal pixel buffering was applied to the NLCD for the selection of hot and cold pixels by using the Focal Density (FD) function in ERDAS Imagine with a 7 × 7 focal window. A 7 × 7 focal window of a uniform land use has FD = 49 at the center pixel; the FD drops to 48 if one pixel in the focal window represents a different land use, 47 for two pixels with a different land use, etc. First, NLCD land use values of 82 (cultivated crops) and 71 (herbaceous) were recoded to 81 (hay/pasture) to encompass agricultural land uses (Allen et al., 2013). Next, the FD function was applied to land use classes in the recoded NLCD for each year of the study with the criterion of FD = 49 for qualification as thermally isolated hot and cold pixels.

Similarly, a 5 × 5 focal window with the NASS CDL and the criterion of FD = 25 were used to define homogenous areas of each of the various crops in the study area. Thus, for example, adjacent corn and soybean fields each have FD = 25 where the crop is homogenous and FD < 25 near the boundary between the fields. With a pixel size of 56 m for the NASS CDL, the buffering distance of 2.5 pixels from the center to the edge of the 5 × 5 focal window is 140 m, thus exceeding the 105 or 120 m buffering distances used by others (Allen et al., 2013; Morton et al., 2013; Clark et al., 2007). An advantage of the FD function compared with the FSD function is that the former does not require the preprocessing step of recoding the twenty to thirty NASS CDL land use numerical designators, which may change from year to year. It could be argued that misclassified pixels within a cropped area could lead to bias in ET estimates if the misclassification was due to poor management (e.g., weed pressures or fertility deficiencies), thereby eliminating low-ET pixels from consideration. On the other hand, in this "prairie pothole" region, numerous small wetlands and low spots within agricultural fields may also contribute to misclassification of agricultural pixels. These small wetlands and depressional areas may have higher ET than the surrounding cropland due to an abundance of water. Thus, either water shortages or excesses may be present within a field. It is beyond the scope of the present work to fully investigate the causes of pixel misclassifications and their effects on ET.

For circular areas defined by the perimeters of center-pivot irrigation systems used in the test project, the inward buffering distance was set at 105 m to isolate irrigated crops from surrounding areas and thereby preclude thermal pixel contamination. Similarly, a buffer of 105 m away from field midlines was used in situations where different crops were present on each half of the field, e.g., site 7 had corn on the north half and soybeans on the south half in 2006.

Model Validation

The performance of the METRIC$_{ND}$ model was assessed by comparison of its ET estimates to ET$_{EC}$ measurements at one site. ET$_{EC}$ measurements were made over irrigated alfalfa from 2 August through 2 October 2007 (60 days) at site 20, station 1, using techniques described by Jia et al. (2009) and Rijal et al. (2012). The major EC instruments consisted of a CSAT3 3D sonic anemometer, KH20 krypton hygrometer, CNR1 Kipp & Zonen net radiometer, Vaisala HMP45 temperature and humidity sensor, HFP01 SC Hukseflux self-calibrating soil heat flux plates, etc. (Campbell Scientific, Logan, Utah). The EC measurement was maintained at 196 cm above the ground. With alfalfa ranging from 12 to 60 cm in height during the experimental period, the EC system for the flux measurement was maintained between 136 and 184 cm. According to the rule of thumb for fetch distance requirement (ASAE, 2004), 136 to 184 m of footprint would be affected when the wind speed is close to neutral condition (<2 m s^{-1}). Therefore, we can say that area measurement with an eddy covariance system was the best choice when comparing to METRIC-derived ET (Wang and Dickinson, 2012).

The QA/QC of the eddy covariance data followed procedures similar to those of Sumner (1996) and Jia et al. (2009). Raw data were corrected for flow distortion and sensor orientation when calculating the sensible flux and latent heat flux to account for associated errors during the measurements, such as coordinate rotation, sonic temperature to air temperature, temperature fluctuations, hygrometer oxygen sensitivity, and separation between the sonic anemometer and the krypton hygrometer. Missing LE values were filled with estimated values using the Priestley-Taylor method. The Bowen ratio method was used to close the energy balance for durations when net radiation values were greater than 0. Daily average ET rates were calculated from the sum of 30 min LE values.

The EC instrumentation location was near the edge of the Landsat 5 TM's scene (P31R26), and the absence of thermal pixels there for some image dates precluded the use of those scenes for comparison of ET$_{EC}$ with ET estimates from METRIC$_{ND}$ (designated ET$_{METRICND}$). It should be noted that the project's selection of a site with alfalfa was beyond our control. One vertex of the AOI was moved 5 km southward to include the EC instrumentation location, and METRIC$_{ND}$ simulations were rerun for P32R26 for frost-free dates during the EC measurement period using the expanded AOI. Comparisons between ET estimates from the pixel overlying the EC system and the ET derived from the EC system were made using mean bias error (MBE), defined as:

$$MBE = ET_{METRICND} - ET_{EC} \quad (10)$$

and mean absolute error (MAE), defined as:

$$MAE = \left| ET_{METRICND} - ET_{EC} \right| \quad (11)$$

Because of limited availability of EC instrumentation within the scope of this project, we also examined ET$_r$F histograms to ensure compliance with constraints recommended by Morton et al. (2013), i.e., that our ET$_r$F values

were within physically realistic constraints. The third approach to model performance assessment was comparison of K_c values derived from $METRIC_{ND}$ with those available in the literature.

ET_rF Interpolation Between Image Dates and Cloud Gap Filling

The third SML module used linear interpolation (Allen et al., 2005) to find daily ET_rF and ET values between successive usable images.

Gap filling of cloud and cloud shadow areas for a given daily ET_rF image was accomplished by time-based linear interpolation daily ET_rF values, where available, from the preceding and successive satellite overpass dates' ET_rF images using the relationship:

$$ET_rF_2 = \frac{\Delta t_2}{(\Delta t_1 + \Delta t_2)} ET_rF_1 + \frac{\Delta t_1}{(\Delta t_1 + \Delta t_2)} ET_rF_3 \quad (12)$$

where Δt_1 is the interval (d) between the preceding and present image dates, and Δt_2 is the interval (d) between the present and subsequent image dates. The ET_rF_1 and ET_rF_3 images represent the ET_rF values for the study area at the preceding and subsequent image dates, respectively. Similarly, linear interpolation was used to obtain daily ET_rF values between consecutive image dates, e.g., between ET_rF_1 and ET_rF_2 or between ET_rF_2 and ET_rF_3. Allen et al. (2012) recommended linear interpolation to fill cloud gaps and suggested curvilinear interpolation to represent periods between gap-filled images. They noted that curvilinear interpolation can become uncertain or speculative when the inter-image intervals become too long because crop development changes appreciably over longer intervals. Other methods of interpolation have been noted in the literature (Long and Singh, 2010; Cammalleri et al., 2014; Semmens et al., 2016; Dhungel et al., 2016).

After cloud gap filling and linear interpolation of ET_rF images were completed in this study, a composite ET_rF image was developed for each growing season. Cloud cover eliminated some images from the modeling process, thus shortening the effective period of simulation with respect to the full growing season. Estimates of ET for daily and longer time periods were calculated by multiplying daily ET_rF values from $METRIC_{ND}$ by ASCE-EWRI (2005) estimates of daily ET_r as calculated from NDAWN data for the Cando station.

Irrigation Effects on ET

Median values of $ET_{METRICND}$ simulations at the test sites were compared with corresponding median $ET_{METRICND}$ estimates for the same time periods and crops in the general study area. Median values were used because they are less sensitive to outliers compared with average values. For both the test sites and the general study area, pixels with NLCD FD values smaller than 49 were excluded from the ET comparisons. Although some of the crops in the study area were irrigated, the larger study area was designated as "rainfed" because irrigated agricultural land comprised a very small percentage of the basin area. The 2006 NASS CDL indicated that the basin was 75% agricultural land (crops such as wheat, corn, soybean, etc.), 11% wetlands, 9% water, 4% urban, and 1% woods. Of the agricultural land, approximately 0.2% was irrigated as computed from the maximum irrigated agricultural area of 1630 ha for 1997 to 2011 (M. Hove, North Dakota State Water Commission, 2012 personal communication; Steele et al., 2015) divided by the agricultural land area. In cases where two or more test sites were available for the same crop and time period, the average of the site median $ET_{METRICND}$ estimates was used for comparison to median $ET_{METRICND}$ estimates for the study area.

Only cloud-free areas (areas with no clouds present or areas in which clouds were removed) were used for ET comparisons. For example, ET was estimated from 20 May through 15 August 2006 for corn at site 6 and the north half of site 7, while clouds on one or more days during this period obscured site 12 and eliminated that site from the analysis. However, additional investigation showed that daily ET for the corn at site 12 could be assessed for 7 July through 15 August 2006 because no clouds eliminated site 12 from consideration. As a result of varying cloud cover for different time periods, the areas of corn available for analysis in the general study area were 4621 and 5180 ha, respectively, for the above two periods. Similar procedures were used for other crops and time periods.

Values of daily ET_r were totaled for comparison with crop-specific $ET_{METRICND}$ totals for corresponding time periods. The resulting period-long K_c values were used to validate the model results. For example, K_c values were expected to approach 1.0 for fully developed, well-watered crops.

The gains in ET attributable to irrigation were computed as the differences between ET at the irrigated test sites ($ET_{Irrigated}$) and ET in the predominantly rainfed study area ($ET_{Rainfed}$) for the same crops and time periods. Linear regression of $ET_{Irrigated}$ versus $ET_{Rainfed}$, pooled across the crops (corn, soybean, spring wheat, and barley) and years (2006, 2007, and 2008) available, was formulated as:

$$ET_{Irrigated} = m \times ET_{Rainfed} + b \quad (13)$$

The slope (m) was used as a measure of the increase in ET associated with irrigation. A t-statistic with n–2 degrees of freedom (df; Miller and Freund, 1977) was used to determine whether the slope (m) was greater than 0, i.e., that ET was significantly increased on the irrigated test sites compared with the same, predominantly rainfed, crops in the larger study area.

Results and Discussion

General Results

No concerns were encountered in the weather data integrity assessment. Application of the ASCE-EWRI weather data integrity assessment techniques confirmed the assessments performed by the HPRCC and NDAWN. The alfalfa field (site 20, station 1), was under frost-free conditions for the period of study, as indicated by a minimum air temperature of -0.5°C, which is higher than the -2.8°C threshold for cold injury to alfalfa (Barnhart, 2012).

Without the energy closure by the Bowen ratio method, 84% of the energy was accounted for in the 30 min measured

flux values when net radiation was greater than 0 and in the scalar factor (ratio of measured LE + H values to $R_r - G$ values). Based on the scalar factor, the unbalanced energy flux was proportionally applied to LE and H based on the Bowen ratio method (Twine et al., 2000). Compared to the 80% average value from more than 50 sites summarized by Wilson et al. (2002), our value was in the acceptable range. During the experimental period, except on 10 August, we did not receive any rainfall that typically caused measurement error for the EC system.

In some Landsat scenes, the albedo, NDVI, and LAI criteria used for selection of cold and hot pixels, coupled with the FD criterion (FD = 49) in the NLCD to ensure thermal pixel buffering, produced few or no hot pixel candidates. We attribute this to the rarity of noncropped or barren agricultural fields in this subhumid region. One approach to address the FD problem could be to allow FD < 49. For example, Allen et al. (2013) addressed land use nonhomogeneity by allowing nonzero FSD values (used similarly to FD in this article to determine land use homogeneity), rather than strictly using FSD = 0. In some instances in this study, tilling of land after cereal crop harvest in mid to late summer produced barren ground, satisfying the albedo, NDVI, LAI, and FD criteria necessary for hot pixels. For fields with cereal crop production, as evident from the NASS CDL, the occurrence of tillage after crop harvest was validated by inspection of at-surface reflectance images.

For some scenes, the cold pixel criteria were relaxed in order to obtain usable simulations. For example, on 8 August 2006, an NDVI value of 0.752 was used for a cold pixel selected at site 6, station A1, for simulation 6. Allen et al. (2012) indicate that NDVI values near 0.7 indicate full or nearly full cover conditions; our field observations confirmed full vegetative cover at the site on this date. The simulation on 3 September 2007 was especially challenging because it produced very few cold pixel candidates throughout the scene. A cold pixel was selected with T_s = 293.3 K, α = 0.193 (within range), NDVI = 0.54, and LAI = 1.1. Tradeoffs occur because other cold pixel candidates were warmer, making it more difficult to obtain $ET_rF < 1.05$ on the upper end of the distribution, e.g., unrealistically high ET_rF values were obtained at site 12 for irrigated corn. On 19 September 2007, the cold pixel ET_rF value was set to 1.0 for simulation 5 because a value of 1.05 was questionable when considering crop senescence at that late date in the season and the lack of irrigation at this cold pixel. The hot pixel criterion of NDVI ≤ 0.15 was relaxed to 0.2 (Allen et al., 2012) for the 28 June 2006 simulations because the original criterion produced only one hot pixel candidate in the study area.

Images late in the season were in some cases not used for ET mapping. For example, the P31R26 image for 25 September 2006 occurred after an earlier frost date, the P31R26 image for 13 August 2008 was very cloudy, and the P32R26 image for 21 September 2008 did not have qualifying cold pixel candidates.

Model Performance

The use of ten iterations of the stability corrections in the H calculations was deemed sufficient to achieve the 0.1% convergence criterion. For example, for the $METRIC_{ND}$ modeling area of this study and an image date of 30 July 2006, the maximum relative change for all pixels in a sensible heat image between the fourth and fifth iterations based on equation 9 was $\Delta H_5 = 0.440\%$, indicating that five iterations would have been insufficient for this case. However, ten iterations gave $\Delta H_{10} = 0.000119\%$. Each successive iteration decreased ΔH_i by a factor of approximately 5 (data not shown). Additional SML coding to stop and exit the iterations when the 0.1% level of convergence is reached may be an area for future work but was not implemented in this study.

Histograms of ET_rF for all image dates for all years are shown in figure 2. All of the selected simulations met the criterion of Morton et al. (2013) of not allowing more than 7.5% of the pixels to have $ET_rF < 0.1$. Most of the simulations met the criterion of not allowing more than 2% of the pixels to have $ET_rF > 1.05$, with the following exceptions. On 30 July 2006, 3.10% of pixels had $ET_rF > 1.05$. A search for a cold pixel candidate yielded only one pixel with $ET_rF > 1.05$ (1.0503), and further simulations were not pursued. On 8 June 2007, 2.06% of pixels had $ET_rF > 1.05$; additional simulations were not pursued. On 11 August 2007, rainfall immediately prior to the image date (12 mm from 6 Aug. through 5:00 a.m. on 11 Aug., including 8.6 mm on 10 Aug.) resulted in ET_rF for the hot pixel of 0.97 according to the FAO-56 model. Although this "wet" image had numerous pixels with $ET_rF > 1.05$ for possible adjustment of the cold pixel, none of the pixels met the cold pixel criteria. Several simulations were tried, including lowering the NLCD focal density criteria from 49 to 37 for thermal pixel buffering, i.e., allowing some mixed land use for cold pixel selection. It was not possible to meet the histogram tail size criteria, i.e., to shift the histogram toward smaller ET_rF values. Difficulty in modeling "wet" images is not unique to METRIC; Sharma et al. (2015) noted poor performance of the Surface Energy Balance System on days with precipitation. For K_c interpolation, we discarded the 11 August 2007 image and interpolated between the prior (2 Aug.) and following (18 Aug.) Landsat 5 TM overpass dates. Morton et al. (2013) noted the omission of scenes whose calibrations did not meet the ET_rF histogram tail size criteria; they noted that such scenes would be removed or recalibrated for use in their final ET estimates. In this study, the resulting time interval is reasonable, i.e., that between two consecutive Landsat 5 TM images for P32R26.

Eddy covariance measurements and $ET_{METRICND}$ estimates are shown in figure 3. While ET_rF values might be expected to continue increasing after the 18 August 2007 satellite image date until the start of the alfalfa cut interval starting on 31 August, the linear interpolation of ET_rF between the 18 August and 3 September satellite image dates shown in figure 3 indicates declining ET_rF after 18 August. Thus, while ET_rF estimates from $METRIC_{ND}$ can be interpolated between successive satellite image dates for continuously growing crops, such interpolations may become inappropriate when they span transition periods from full cover to recently cut alfalfa. For comparison purposes, the alfalfa cut interval was avoided by excluding data from 19 August

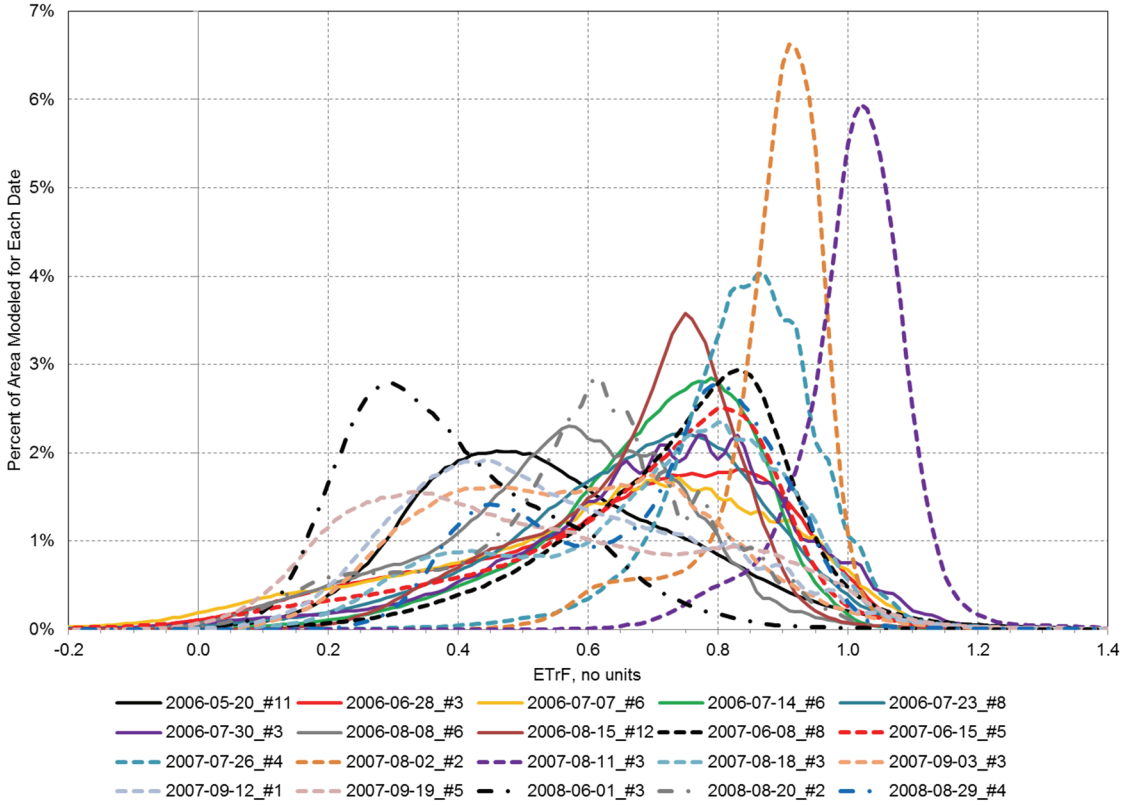

Figure 2. Histograms of fraction of reference ET (ET_rF) for $METRIC_{ND}$ scenes. Legend entries are dates and simulation numbers, e.g., 2006-05-20_#11 is 20 May 2006, simulation number 11.

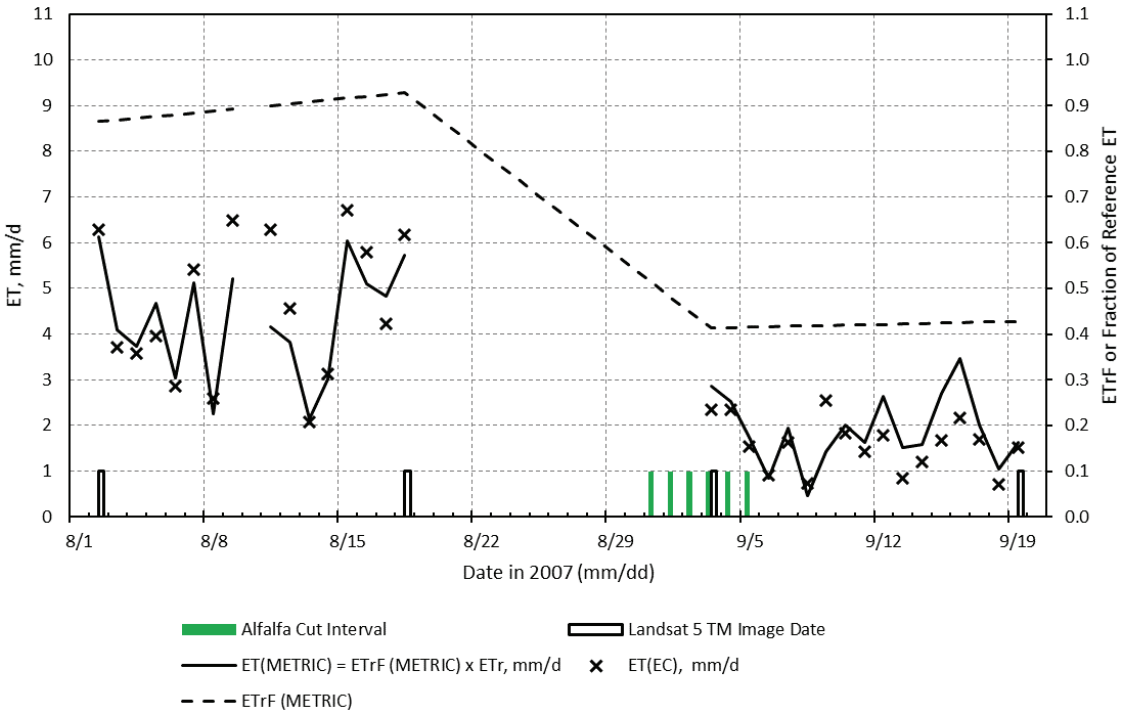

Figure 3. Comparison of estimates of evapotranspiration (ET) from eddy covariance measurements [ET(EC)] and METRIC [ET(METRIC)] over irrigated alfalfa from 2 August through 19 September 2007 at site 20, station A1. Data from 10 August are omitted due to unavailability of eddy covariance data. The alfalfa cut intervals indicate cutting between 31 August and 5 September; daily site visits were not possible.

through 2 September. Figure 3 indicates that $METRIC_{ND}$ tended to underestimate ET for the higher ET values when alfalfa was uncut (MBE = -0.3 mm d^{-1} and MAE = 0.5 mm d^{-1} for 2 to 18 Aug.) and overestimate ET for the lower ET values after cutting (MBE = 0.3 mm d^{-1} and MAE = 0.5 mm d^{-1} for 3 to 19 Sept.). This conclusion is supported by the

linear regression relationship $ET_{METRICND} = 0.785ET_{EC} + 0.668$ with $R^2 = 0.88$, which shows a strong correlation between the two methods. This is similar to the findings of Liebert et al. (2015) of $ET_{METRIC} = 0.86ET_{EC} + 0.4$ with $R^2 = 0.86$. Under- and overestimations of ET tended to cancel out for the whole measurement period, with MBE = 0.01 mm d^{-1} and MAE = 0.51 mm d^{-1} for 2 August through 19 September (excluding 10 Aug. and 19 Aug. through 2 Sept.).

Average tensiometer readings in the 70 to 80 kPa range on several dates (data not shown) indicated that the alfalfa was generally not well watered across site 20. Furthermore, some tensiometer readings were not available due to dry soil conditions and loss of water from the tensiometers. For fully irrigated alfalfa, $ET_rF \approx 1.0$ or slightly higher would be expected. However, the farmer at this site expressed concerns about wheel ruts from the irrigation system and hence applied irrigation amounts that were smaller than we requested. As a result, ET_rF values smaller than 1.0 for uncut alfalfa would be expected and were predicted by the $METRIC_{ND}$ simulations for site 20 (fig. 3).

IRRIGATION EFFECTS ON ET

Table 4 summarizes periodic ET estimates from $METRIC_{ND}$ for the available crops and time periods at the test sites and the corresponding, predominantly rainfed crops in the study area. Sites 1, 2A, and 20 were outside the original study area footprint (fig. 1), while sites 35 and 36 were too small to have any remaining area for analysis after thermal pixel and land use buffering.

The increases in ET associated with irrigation ranged from 3 mm for corn for the 10-day period of simulation in 2008 to 146 mm for the 88-day period of simulation in 2006. The increases in ET under irrigation averaged 30%, 20%, and 18% for 2006, 2007, and 2008, respectively. The year-by-year variation is consistent with the results anticipated by Steele et al. (2015), who noted that 2006 was the hottest and driest year in the 1995-2008 period, i.e., 2006 had the highest potential for the addition of irrigation.

For all simulations, crop ET was smaller than ET_r, i.e., $ET_rF < 1.0$ for all crops and time periods simulated. The trends in ET_rF are also consistent with crop development in the region. For corn and soybean, ET_rF averaged 0.76 and 0.56, respectively, for the 88-day period beginning on 20 May 2006, while the ET_rF values increased to 0.91 and 0.89, respectively, for the 40-day period beginning on 7 July 2006. The longer period encompassed crop emergence in late May, whereas the shorter period encompassed more fully developed stages of crop growth.

The 10-day ET_rF values of 0.90, 0.86, and 0.98 for corn, spring wheat, and soybean approach 1.0 for the period starting on 20 August 2008. For comparison, Steele et al. (1996) found a peak "days past planting" K_c (or ET_rF) value of 0.96 for irrigated corn in southeastern North Dakota. The Penman reference ET equation employed in that study (Allen, 1986) was developed prior to the ASCE-EWRI method. The ET_rF value of 0.86 for wheat in 2008 is somewhat smaller, likely due to crop maturation and senescence, although its 27 May emergence at site 13 (Steele and Hopkins, 2010) was somewhat late. The lower ET_rF for corn compared with soybean might be attributed to corn's lower salt tolerance. Rhoades and Loveday (1990) list salt tolerance thresholds of 1.7 dS m^{-1} for corn, 5.0 dS m^{-1} for soybean, and 6.0 dS m^{-1} for wheat. Hopkins and Steele (2011) noted that "seven of the 10 sites" in the test project "had soils that were strongly influenced by capillary rise of salts from the groundwater."

Equation 13 is plotted in figure 4 using the ET averages for the irrigated test sites ($ET_{Irrigated}$) and the median ET estimates for the predominantly rainfed crops in the study area

Table 4. Summary of periodic ET estimates from METRIC for selected crops in the Devils Lake basin and at selected irrigated test sites.

	2006						2007				2008			
Simulation start date	20 May	20 May	7 July	7 July	7 July		8 June	8 June	8 June		20 Aug.	20 Aug.	20 Aug.	
Simulation end date	15 Aug.	15 Aug.	15 Aug.	15 Aug.	15 Aug.		12 Sept.	12 Sept.	12 Sept.		29 Aug.	29 Aug.	29 Aug.	
Days (includes start and end dates)	88	88	40	40	40		97	97	97		10	10	10	
Crop	Corn	Soybean	Corn	Soybean	Spring wheat		Corn	Barley	Spring wheat		Corn	Spring wheat	Soybean	
Median ET for crop in study area (mm)	296	300	190	181	180		348	346	387		45	34	44	
Crop area available for analysis (ha)	4621	15778	5180	17103	45153		5007	6386	34778		5593	45825	15802	
Test Site	Median ET at Test Site (mm)					Area, (ha)[a]	Median ET at Test Site (mm)			Area, (ha)[a]	Median ET at Test Site (mm)			Area, (ha)[a]
6	434	-	-	-	-	24.0	328	-	-	23.5	50	-	-	24.0
7 (north)	450	-	-	-	-	6.9	-	-	-	-	-	-	-	-
7 (south)	-	323	-	-	-	6.9	-	-	-	-	-	-	-	-
7 (all)	-	-	-	-	-	-	380	-	-	13.8	43	-	-	10.8
12	-	-	253	-	-	20.7	424	-	-	20.7	47	-	-	26.3
13 (north)	-	-	-	-	-	-	484	-	-	1.4	-	45	-	8.8
13 (south)	-	-	-	-	240	5.8	-	-	-	-	49	-	-	8.1
18 (east)	-	-	-	238	-	9.6	-	-	491	4.5	-	-	51	4.5
18 (west)	-	-	235	-	-	9.5	-	407	-	5.6	50	-		5.6
ET averages for test sites	442	323	244	238	240		404	407	491		48	45	51	
ET gain under irrigation (mm)	146	23	54	57	60		56	61	104		3	11	7	
(%)	49%	8%	28%	31%	33%		16%	18%	27%		7%	32%	16%	
$ET_{r\ ASCE\text{-}EWRI}$ from Cando NDAWN (mm)	579	579	267	267	267		527	527	527		53	53	53	
ET_rF (= $ET_{Test\ Sites}/ET_{r\ ASCE\text{-}EWRI}$)	0.76	0.56	0.91	0.89	0.90		0.77	0.77	0.93		0.91	0.86	0.97	

[a] Irrigated area at each site minus thermal pixel buffering inward from each center pivot border and buffering away from midlines in dual-cropped fields, where applicable.

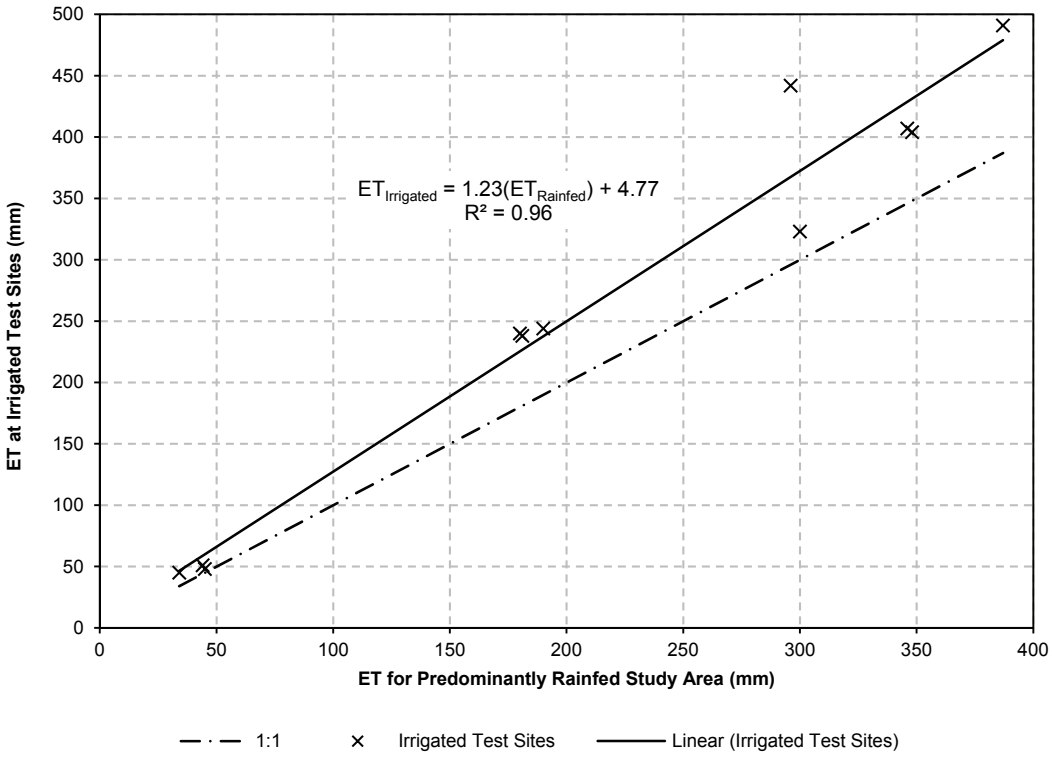

Figure 4. Estimated evapotranspiration gains under irrigation in the study area. Crops under comparison were corn, soybean, and spring wheat in 2006; corn, barley, and spring wheat in 2007; and corn, spring wheat, and soybean in 2008.

($ET_{Rainfed}$) from table 4. The figure shows a strong correlation ($R^2 = 0.96$) between $ET_{Irrigated}$ and $ET_{Rainfed}$. The largest departures from the regression line occur at approximately 300 mm of ET. The ($ET_{Rainfed}$, $ET_{Irrigated}$) point (296, 442) is conspicuously above the line and corresponds with corn at sites 6 and 7 in 2006. Agronomic and irrigation practices to maximize yield would generally be associated with high ET values. In other studies in North Dakota, Stegman (1982, 1986, 1989) reported direct relationships between yield and ET for corn and soybean. The ($ET_{Rainfed}$, $ET_{Irrigated}$) point (300, 323) in figure 4 is markedly below the regression line and corresponds with soybean in the south half of site 7 in 2006. There are two soil map units in the south half of site 7 (not listed in table 1) that are not found (or are minimally present at the edge of the irrigated area) in the north half of the field (USDA-NRCS, 2011). Map unit F612C occupies 4.82% of the site, is Barnes-Buse very stony loams, with 3% to 9% slopes, and would contain an abundance of free carbonates and therefore be expected to stunt soybean growth. Map unit F100A occupies 17.69% of the site, is Hamerly-Tonka complex, and has more Hamerly than Tonka; the Hamerly will tend to generate iron deficiency chlorosis in soybean. The total of 22.5% of site 7 in these soil map units would be expected to depress the soybean yield and the corresponding ET for the south half of the field. It is uncertain why ET was depressed at site 6 in 2007 (table 4). The ET map indicated generally lower ET under the center-pivot irrigation system at the site compared with the surrounding rainfed soybean and sunflower crops identified in the NASS CDL. Field notes from a project worker indicated that station A1 was inaccessible on 15 August 2007 because 15 cm of standing water was present on the soil surface. Whether excessively wet conditions persisted long enough across the field at a severity level sufficient to depress yield and ET is unknown. Detailed and frequent (subweekly) crop and soil monitoring site visits would have been desirable but were beyond the scope of this project. A t-statistic for the slope of (m) of $ET_{Irrigated}$ versus $ET_{Rainfed}$ in equation 13 was 5.511, which exceeds the critical value of 4.297 for 9 df at the 0.001 level of significance, leading to the conclusion that $m > 0$. The physical interpretation is that irrigation produced an approximately 23% gain in ET for this study.

Applying the gains in ET to the flood mitigation objective, a 23% increase in a seasonal ET of 348 mm (median corn ET in the study area in 2007; table 4), for example, for rainfed crops in the study area would be 80 mm of additional ET. This is smaller than the 137 mm or 36% gain in ET for irrigated crops estimated by Bartlett and West (2002), who used a one-dimensional soil water balance model for 1992-2001 and the methods summarized by Steele et al. (2015) to estimate ET of 380 mm for a rainfed crop mix in the Devils Lake basin. The 137 mm of additional ET estimated by Bartlett and West (2002) was projected as equivalent to 45,600 ha-m year^{-1} (370,000 acre-ft year^{-1}) of water removal from the basin under their assumptions of crop mixes, land selection, proximity to water sources, etc. Using a simple proportion, the 80 mm of additional ET estimated in this study would represent approximately 26,600 ha-m year^{-1} (216,000 acre-ft year^{-1}) of water removal from the basin. Users of these estimates must fully understand the assumptions about soil irrigability, particularly internal soil drainage, made by Bartlett and West (2002). The baseline ET for rainfed crops

in the Bartlett and West (2002) study was likely lower than the rainfed crop ET estimates in this study because the modeling approach in the former study did not consider contributions to ET from shallow groundwater (as noted by Steele et al., 2015). Shallow groundwater depths with probable contributions to ET were observed at several sites in this study (table 1), and this ET would be detected by the METRIC$_{ND}$ process.

On the other hand, the relative increases in ET for irrigated crops in this study are larger than the relative increases in ET estimated by SEBAL (Steele et al., 2015) for irrigated corn in 2006 at sites 6, 7, 12, and 18 in the Devils Lake basin (both studies used the same site designations). In that study, the average ET for corn in the predominantly rainfed basin was estimated at 435 mm for May through September, with irrigated site averages that were 40 mm (9%) and 62 mm (14%) higher for sites 6 and 7, respectively, and 6 mm (1%) and 41 mm (9%) lower for sites 12 and 18, respectively; the area-weighted ET gain was 17 mm or 4% for these irrigated corn sites. The lower ET at site 18 was attributed to high levels of soil salinity. The ET gain for irrigation was reported as 33 mm or 8% by Steele et al. (2015) when all irrigated crops in their study were compared with ET for predominantly rainfed spring wheat, which ranked first in crop area in 2006 in the Devils Lake basin. A conclusion of that study was that switching to longer-season crops (corn instead of wheat) would be a more effective means of increasing ET as a flood mitigation tool.

The smaller relative increases in ET in the SEBAL study (Steele et al., 2015) compared with this study may be partly attributable to a damping effect via the inclusion of ET estimation for early May and late September in the SEBAL study. The peak months for irrigation in this region are typically June, July, and August, and the contrasts between irrigated and rainfed crop ET would be expected to be smaller for May and September. For example, the SEBAL study used the 20 May 2006 Landsat 5 image to represent the entire month of May, whereas in this study, the 20 May 2006 Landsat 5 image was not used for 1-19 May (see tables 3 and 4). Corn emergence dates in 2006 were 14, 21, 26, and 27 May at sites 6, 7, 12, and 18, respectively (Steele et al., 2015). The site operators followed the region's typical practice of not applying preplant irrigations because they already faced the risk that the high spatial and temporal variability of rainfall would cause trafficability problems for planting operations. These factors led to the conclusion that there would have been little or no differences in ET for irrigated versus rainfed fields during at least the first half of May. Similar comparisons could be made for late September; irrigation events become less frequent late in the season with crop maturation and energy cost considerations, as well as with concerns about trafficability for harvest operations. These analyses underscore the importance of understanding the interpolation and/or extrapolation methods employed in ET estimation methods, as well as their limitations and implications for water management.

In a preliminary study using SEBAL in the Boise Valley of Idaho, Morse et al. (2003) estimated ET irrigated crops at 276 mm or 51% more than "other agriculture" (812 mm vs. 536 mm) in 2000. The larger ET for irrigated crops was most likely due to the semi-arid environment there, with only 20 to 30 cm of annual precipitation. Irrigated crops comprised 45% of the land use/land cover types in their study (excluding water), which is in sharp contrast with 0.2% in this study. Furthermore, the data from Morse et al. (2003) indicated that 95% of land uses associated with agriculture were irrigated.

Although there appears to be the potential for increased ET with irrigation in the Devils Lake basin, we were concerned about the project's feasibility even before it was undertaken because generalized soil information indicated that the proportion of irrigable soils was (and is) quite low, according to GIS analysis of generalized soil units (NRCS STATSGO digital data; USDA-NRCS, 2011). When soil map units are listed in order of cumulative percentage, about 85.5% of the area is eliminated before a map unit is encountered that has at least one component rated as an irrigable soil, according to the 1982 North Dakota Irrigation Guide (USDA-SCS, 1982). Over 91.7% of the area is eliminated before a generalized soil map unit is found where each soil component is classified as an irrigable soil. During the site selection process, the DLBJWRB's consulting firm found that most of the sites under consideration for the DLBWUTP have somewhat poorly drained soils or some combination of soil map units including sodium-affected soils that would be expected to exhibit problems under irrigation. Other apparent problems involve the total area of irrigable (or conditionally irrigable) soils that would lie under center-pivot irrigation systems, i.e., small inclusions of irrigable soils among larger areas of nonirrigable soils might not warrant full-sized irrigation systems. Despite these limitations, the North Dakota State Water Commission was under pressure to find ways to remove excess water from the basin. While acknowledging the limited area of irrigable soils, the North Dakota State Water Commission desired to have quantifiable estimates of potential gains (or not) in ET under irrigated versus rainfed conditions in the basin, and this project was conducted for that purpose.

Our field experience in the DLBWUTP confirmed that applying high seasonal irrigation totals to achieve increased ET in the basin could be very problematic for drainage and trafficability of the field sites. As noted by Steele et al. (2015), one of the site operators noted very wet field conditions in the spring of 2007 following the 254 mm of irrigation applied in 2006. Thus, careful management of irrigation and drainage would be required if irrigation were to be pursued as a flood mitigation strategy for the basin. Subsurface drainage was excluded from the inception and design of the DLBWUTP. However, future installation of subsurface drainage systems and water removal networks, such as drainage ditches, may make it worthwhile to revisit the gains in ET attainable with irrigation. While subsurface drainage could alleviate problems such as waterlogging and poor soil trafficability, disposal of drainage water and possible salinity concerns associated with drainage water would also need to be addressed. Drip irrigation might address the trafficability problem, but its higher application efficiency contradicts the water disposal or "water wasting" objective of this project. In addition, drip irrigation is typically significantly more expensive than sprinkler irrigation.

Variations in ET by soil type were not analyzed in this

study. Steele et al. (2015) noted that modest gains in ET would be possible on coarse-textured soil map units in the study area. However, the proportion of sandy loam and loamy sand map units is relatively small, and these units are scattered throughout the basin, making it difficult to justify investment in irrigation machines for the small areas available.

Yield versus ET analyses were beyond the scope of the present study and would have required access to yield data from the farmer-cooperators at the test sites and from farmers outside the project in the larger basin area. It would have been helpful to have had access to agronomic consultations during the project to assess the potential and actual impacts of excessive irrigation on crop productivity, health, disease, etc. That is, the sustainability of excess irrigation for flood mitigation purposes was not addressed in this study.

Estimates of $ET_{METRICND}$ from this study and estimates of ET_{SEBAL} based on Steele et al. (2015) for selected crops and time periods in 2006 are compared in table 5. The averages of estimated gains in ET for irrigated versus rainfed crops were 28% for $METRIC_{ND}$ and 14% for SEBAL. The average ratios of $ET_{METRICND}/ET_{SEBAL}$ for each time period and crop combination are approximately 1.25 for the predominantly rainfed crops in the study area and 1.42 at the irrigated test sites. The differences between $ET_{METRICND}$ and ET_{SEBAL} may be associated with the calibration or validation methods used in each study. For the $METRIC_{ND}$ modeling, further study would be required to assess whether the use of $ET_rF = 1.05$ for cold pixels was appropriate or may have resulted in some overestimation of ET. On the other hand, comparisons of the histograms of ET_rF for $METRIC_{ND}$ (fig. 2), the $ET_{METRICND}$ comparisons with ET_{EC} at site 20 (fig. 3), and the $METRIC_{ND}$ ET_rF values near 1.0 for 7 July through 14 August (table 5) suggest that $METRIC_{ND}$ provided reasonable ET estimates. Validation of the ET_{SEBAL} estimates was based on comparing ASCE-EWRI ET_o values to the 97th percentile of ET_{SEBAL} for grassland and pasture land uses in the SEBAL study area. BREB or EC instrumentation was not used to validate the ET_{SEBAL} values, making parallel comparisons with this study difficult. Based on Ref-ET calculations for the Cando NDAWN station, the ET_r/ET_o ratio for the periods 1 June through 14 August and 17 July through 14 August (the simulation periods in table 5) and for 1 May through 30 September (the growing season for the SEBAL study) were 1.30, 1.30, and 1.33, respectively.

Additional Research

Future studies could be directed toward improved methods for selection of hot and cold pixels. For example, during mid-season, hot pixels are difficult to find because virtually all agricultural land is cropped in this subhumid to semi-arid region. By late August and September, small grains have been harvested, and in some cases the land has been tilled, providing hot pixel candidates. Relaxing the upper limit in the NDVI criterion ($0.10 \le NDVI \le 0.15$) to 0.20 (Allen et al., 2012) was helpful in finding hot pixel candidates in this study. Assuming that hot pixel candidates are available (i.e., they meet the α, NDVI, and LAI criteria), future work may focus on using SSURGO data to select hot pixel candidates from coarse-textured soils whenever possible to minimize the effects of residual soil evaporation compared with loams and clays at the hot pixel. Purposely creating barren agricultural plots reserved as potential hot pixel candidates has been discussed as a possible strategy for future studies (W. Schuh, North Dakota State Water Commission, 2008 and 2016 personal correspondence), but sponsorship and maintenance

Table 5. Comparison of METRIC and SEBAL ET estimates for selected time periods and crops in 2006.

Simulation Date Ranges, Crops, Models, and Evapotranspiration Results											
Simulation start date	1 June				17 July						
Simulation end date	14 August				14 August						
Days (including start and end dates)	75				29						
Crop	Corn		Soybean		Corn		Soybean		Spring Wheat		
Model (M = $METRIC_{ND}$ and S = SEBAL)	M	S	M	S	M	S	M	S	M	S	
Median ET for crop in study area (mm)	298	251	302	210	135	116	133	110	116	95	
Crop area available for analysis (ha)	4621	5174	15778	18297	5180	5861	17103	19868	45153	52502	
Test Site	Median ET at Test Site (mm)										Area (ha)[a]
6	409	301	-	-	-	-	-	-	-	-	24.0
7 (north)	417	306	-	-	-	-	-	-	-	-	6.9
7 (south)	-	-	300	191	-	-	-	-	-	-	1.7
12	-	-	-	-	190	134	-	-	-	-	20.7
13 (south)	-	-	-	-	-	-	-	-	176	131	5.8
18 (east)	-	-	-	-	-	-	190	131	-	-	4.5
18 (west)	-	-	-	-	174	136	-	-	-	-	5.6
ET averages for test sites	413	303	300	191	182	135	190	131	176	131	
ET gain under irrigation (mm)	115	52	-2	-19	47	19	57	21	60	36	
ET gain under irrigation (%)	39%	21%	-1%	-9%	35%	16%	43%	19%	51%	38%	
$ET_{r\ ASCE\text{-}EWRI}$ from Cando NDAWN (mm)	495		495		184		184		184		
ET_rF (= $ET_{Test\ Sites}/ET_{r\ ASCE\text{-}EWRI}$)	0.83	0.61	0.61	0.39	0.99	0.73	1.03	0.71	0.96	0.71	

[a] Irrigated area at each test site minus thermal pixel buffering inward from each center pivot border and buffering away from midlines in dual-cropped fields, where applicable.

requirements remain to be addressed. Such hot pixel plots would ideally be located near existing NDAWN weather stations and be situated on relatively high terrain to avoid or minimize wet conditions. This study's simulations did not use $0.05 \leq ET_rF \leq 0.15$, as proposed by Allen et al. (2012), for residual soil moisture evaporation at the hot pixel up to several weeks after significant rainfall events. The additional research on soil water characteristics, tillage and cropping history, etc., required for this avenue of inquiry was beyond the scope of the present study.

The change in H values at each pixel could be tested within each iteration of the loop in the SML code for atmospheric stability corrections with the aim of terminating the loop early if sufficient convergence is obtained. In contrast, the current approach uses ten iterations regardless of whether sufficient convergence is obtained earlier, e.g., on the eighth or ninth iteration.

In raster-based modeling environments, further use of FD in the NLCD should be investigated for thermal pixel buffering, as it appears to have advantages compared with FSD. First, FD provides a straightforward representation of the homogeneity of land use. For example, a 7×7 focal window with FD = 48 is 48/49ths or 98% homogeneous; FSD offers only a generalized interpretation of homogeneity. Second, FD provides a physical basis for suggesting minimum or threshold FD values. For example, for a 7×7 focal window, we plotted histograms of pixel counts versus focal densities and observed "spikes" at FD values of 42, 35, 28, etc. (data not shown) because these values indicate that an edge column or an edge row of pixels in the focal window has a different land use compared with the center pixel. In terms of the rectangular land unit layouts in the northern Great Plains, FD = 49 in the NLCD indicates homogenous land use in the middle of a field, FD = 42 suggests that one edge row or column of pixels in the focal window is likely occupied by a road or a field boundary, FD = 35 indicates two edge rows or columns of pixels possess a different classification compared with the center pixel, etc. This analysis further suggests that FD ≥ 43 likely ensures homogeneity of agricultural land use while allowing random errors of individual pixel misclassifications. Similar analyses could be applied to other focal window sizes as needed. In addition, different FD criteria could be applied to cold and hot pixels, e.g., the more stringent FD = 49 could be used for the more abundantly occurring pixels meeting the cold pixel criteria in this region, while lower FD values might be applied to the hot pixel criteria. Third, FD is more robust than FSD, i.e., FD is independent of the particular numbers used to label land use classes. That is, reassigning the numbers used to label land use classes would likely change the FSD values but would not change the FD values.

The use of annual rather than five-year land use classifications may further improve the thermal pixel buffering process for ET mapping. For example, the NASS CDL may more accurately represent the extent of water bodies that fluctuate from year to year in our "prairie pothole" region, tree groves that may be removed or planted, etc., compared with the five-year cycle of NLCD images. A trade-off in using annual versus five-year images is the pixel size of each, i.e., thermal pixel buffer distances should be re-examined if alternatives to the NLCD are used in future studies.

Estimation of effective rainfall and irrigation could be considered. In a "water wasting" project such as this, it would be desirable to know the efficiency with which pumped water reaches the crop root zone.

Use of Landsat 7 images could have been incorporated into this study, especially for 2008 when few Landsat 5 images were usable. However, the present study provides a variety of simulation durations, locations, soil types, crops, and years, thereby enabling robust estimates of the effects of irrigation on ET.

Ideally, EC or BREBS equipment would have been available and used for all years in the project to validate the ET estimates for all of the images used.

Recording of emergence and harvest dates of irrigated and rainfed crops would be desirable to improve the comparability of the fields used for analysis. However, this would necessitate far more field monitoring and may only be realistic for research within an experiment station site rather than for general field sites spread across the countryside. Development of K_c curves using procedures similar to those of Singh and Irmak (2009) may be an area for future research.

Conclusions

The METRIC model was adapted and applied to three years of Landsat 5 data in the Devils Lake basin in northeastern North Dakota. Estimates of ET were compared for irrigated and rainfed crops in the basin. It appears there is potential for irrigation to increase crop ET by 23%, thereby providing some flood mitigation possibilities through disposal of excess water. However, drainage, salinity, and sodium concerns markedly limit the availability of land for irrigation in the basin. Subsurface drainage may be required to remove excess water from the soil profile, and drainage will likely be attended by additional problems with regard to salinity.

Acknowledgements

This study was supported by the North Dakota State Water Commission and the North Dakota Agricultural Experiment Station. The Devils Lake Basin Water Utilization Test Project was supported by the Devils Lake Basin Joint Water Resource Board, the North Dakota State Water Commission, and the USDA Natural Resources Conservation Service. Use of trade names is for informational purposes only, and no endorsement is implied by the authors nor by North Dakota State University. We thank numerous individuals for their contributions to this study, including James Moos, Ramesh Gautam, David Kirkpatrick, Rodney Utter, Jana Daeuber, and Lori Buckhouse.

References

Allen, R. G. (1986). A Penman for all seasons. *J. Irrig. Drain. Eng., 112*(4), 348-368. https://doi.org/10.1061/(ASCE)0733-9437(1986)112:4(348)

Allen, R. G. (2002). Ref-ET: Reference evapotranspiration calculation software for FAO and ASCE standardized equations.

Kimberly, ID: University of Idaho. Retrieved from http://extension.uidaho.edu/kimberly/tag/reference-evapotranspiration/

Allen, R. G. (2011). Skin layer evaporation to account for small precipitation events: An enhancement to the FAO-56 evaporation model. *Agric. Water Mgmt., 99*(1), 8-18. http://dx.doi.org/10.1016/j.agwat.2011.08.008

Allen, R. G., Burnett, B., Kramber, W., Huntington, J., Kjaersgaard, J., Kilic, A., ... Trezza, R. (2013). Automated calibration of the METRIC-Landsat evapotranspiration process. *JAWRA, 49*(3), 563-576. https://doi.org/10.1111/jawr.12056

Allen, R. G., Pereira, L. S., Howell, T. A., & Jensen, M. E. (2011). Evapotranspiration information reporting: I. Factors governing measurement accuracy. *Agric. Water Mgmt., 98*(6), 899-920. http://dx.doi.org/10.1016/j.agwat.2010.12.015

Allen, R. G., Pereira, L. S., Raes, D., & Smith, M. (1998). Crop evapotranspiration: Guidelines for computing crop water requirements. Irrigation and Drainage Paper No. 56. Rome, Italy: United Nations FAO.

Allen, R. G., Tasumi, M., & Trezza, R. (2005). METRIC: Mapping evapotranspiration at high resolution: Applications manual for Landsat satellite imagery. Ver. 2.0. Kimberly, ID: University of Idaho.

Allen, R. G., Tasumi, M., & Trezza, R. (2007a). Satellite-based energy balance for mapping evapotranspiration with internalized calibration (METRIC): Model. *J. Irrig. Drain. Eng., 133*(4), 380-394. https://doi.org/10.1061/(ASCE)0733-9437(2007)133:4(380)

Allen, R. G., Tasumi, M., Morse, A., Trezza, R., Wright, J. L., Bastiaanssen, W., ... Robison, C. W. (2007b). Satellite-based energy balance for mapping evapotranspiration with internalized calibration (METRIC): Applications. *J. Irrig. Drain. Eng., 133*(4), 395-406. https://doi.org/10.1061/(ASCE)0733-9437(2007)133:4(395)

Allen, R. G., Trezza, T., Tasumi, M., & Kjaersgaard, J. (2012). Mapping evapotranspiration at high resolution using internalized calibration: Applications manual for Landsat satellite imagery. Ver. 2.0.8. Kimberly, ID: University of Idaho.

Anderson, M. C., Neale, C. M. U., Li, F., Norman, J. M., Kustas, W. P., Jayanthi, H., & Chavez, J. (2004). Upscaling ground observations of vegetation water content, canopy height, and leaf area index during SMEX02 using aircraft and Landsat imagery. *Remote Sens. Environ., 92*(4), 447-464. http://dx.doi.org/10.1016/j.rse.2004.03.019

ASAE. (2004). EP505: Measurement and reporting practices for automatic agricultural weather stations. St. Joseph, MI: ASAE.

ASCE-EWRI. (2005). *The ASCE standardized reference evapotranspiration equation*. R. G. Allen, I. A. Walter, R. L. Elliot, T. A. Howell, D. Itenfisu, M. E. Jensen, & R. L. Snyder (Eds.). 0-7844-0805-X. Reston, VA: ASCE Environmental and Water Resources Institute.

Barnhart, S. (2012). Cold injury to alfalfa. Ames, IA: Iowa State University. Retrieved from http://crops.extension.iastate.edu/cropnews/2012/04/cold-injury-alfalfa

Bartlett and West. (2002). *Devils Lake upper basin water utilization and management: Reconnaissance level investigation*, Vol. 1. Bismarck, ND: Bartlett and West Engineers, Inc.

Bastiaanssen, W. G. M (2000). SEBAL-based sensible and latent heat fluxes in the irrigated Gediz Basin, Turkey. *J. Hydrol., 229*(1), 87-100. http://dx.doi.org/10.1016/S0022-1694(99)00202-4

Bastiaanssen, W. G. M, Menenti, M., Feddes, R. A., & Holtslag, A. A. M. (1998a). The surface energy balance algorithm for land (SEBAL): 1. Formulation. *J. Hydrol., 212-213*, 198-212. http://dx.doi.org/10.1016/S0022-1694(98)00253-4

Bastiaanssen, W. G. M, Pelgrum, H., Wang, J., Ma, Y., Moreno, J. F., Roerink, G. J., & van der Wal, T. (1998b). The surface energy balance algorithm for land (SEBAL): 2. Validation. *J. Hydrol., 212-213*, 213-229. http://dx.doi.org/10.1016/S0022-1694(98)00254-6

Bastiaanssen, W. G. M, Noordman, E. J., Pelgrum, H., Davids, G., Thoreson, B. P., & Allen, R. G. (2005). SEBAL model with remotely sensed data to improve water resources management under actual field conditions. *J. Irrig. Drain. Eng., 131*(1), 85-93. https://doi.org/10.1061/(ASCE)0733-9437(2005)131:1(85)

Cammalleri, C., Anderson, M. C., Gao, F., Hain, C. R., & Kustas, W. P. (2014). Mapping daily evapotranspiration at field scales over rainfed and irrigated agricultural areas using remote sensing data fusion. *Agric. Forest Meteorol., 186*(15), 1-11. https://doi.org/10.1016/j.agrformet.2013.11.001

Chander, G., Markham, B. L., & Helder, D. L. (2009). Summary of current radiometric calibration coefficients for Landsat MSS, TM, ETM+, and EO-1 ALI sensors. *Remote Sens. Environ., 113*(5), 893-903. http://dx.doi.org/10.1016/j.rse.2009.01.007

Chavez, J. L., Gowda, P. H., Howell, T. A., Garcia, L. A., Copeland, K. S., & Neale, C. M. (2012). ET mapping with high-resolution airborne remote sensing data in an advective semiarid environment. *J. Irrig. Drain. Eng., 138*(5), 416-423. https://doi.org/10.1061/(ASCE)IR.1943-4774.0000417

Clark, B., Soppe, R., Lal, D., Thoreson, B., Bastiaanssen, W., & Davids, G. (2007). Variability of crop coefficients in space and time: Examples from California. *Proc. 4th Intl. USCID Conf.* (pp. 3-6). Denver, CO: U.S. Commission on Irrigation and Drainage.

Dhungel, R., Allen, R. G., Trezza, R., & Robison, C. W. (2016). Evapotranspiration between satellite overpasses: Methodology and case study in agricultural dominant semi-arid areas. *Meteorol. Appl., 23*(4), 714-730. https://doi.org/10.1002/met.1596

ERDAS. (2010). *ERDAS spatial modeler language reference manual*. Norcross, GA: ERDAS, Inc.

Hopkins, D. G., & Steele, D. D. (2011). Devils Lake basin water utilization test project: Soil sustainability investigations. Fargo, ND: North Dakota State University.

Hubbard, K. G. (2001). Multiple station qualitative procedures. In K. G. Hubbard & M. V. Sivakumar (Eds.), *Proc. Intl. Workshop on Automated Weather Stations for Applications in Agriculture and Water Resources Management: Current Use and Future Perspectives* (pp. 133-136). Lincoln, NE: High Plains Climate Center, and Geneva, Switzerland: World Meteorological Organization.

Jia, X., Dukes, M. D., & Jacobs, J. M. (2009). Bahiagrass crop coefficients from eddy correlation measurements in central Florida. *Irrig. Sci., 28*(1), 5-15. https://doi.org/10.1007/s00271-009-0176-x

Liebert, R., Huntington, J., Morton, C., Sueki, S., & Acharya, K. (2016). Reduced evapotranspiration from leaf beetle induced tamarisk defoliation in the Lower Virgin River using satellite-based energy balance. *Ecohydrol., 9*(1), 179-193. https://doi.org/10.1002/eco.1623

Long, D., & Singh, V. P. (2010). Integration of the GG model with SEBAL to produce time series of evapotranspiration of high spatial resolution at watershed scales. *J. Geophys. Res.: Atmos., 115*(D21). https://doi.org/10.1029/2010JD014092

Meek, D. W., & Hatfield, J. L. (2001). Single station quality control procedures. K. G. Hubbard & M. V. Sivakuma (Eds.), *Proc. Intl. Workshop on Automated Weather Stations for Applications in Agriculture and Water Resources Management: Current Use and Future Perspectives* (pp. 123-132). Lincoln, NE: High Plains Climate Center, and Geneva, Switzerland: World Meteorological Organization.

Miller, I., & Freund, J. E. (1977). Inferences based on the least-squares estimators. In *Probability and statistics for engineers* (pp. 295-302). Englewood Cliffs, NJ: Prentice-Hall.

Morse, A., Kramber, W. J., Wilkins, M., Allen, R. G., & Tasumi, M. (2003). Preliminary computation of evapotranspiration by land cover type using Landsat TM data and SEBAL. *Proc. IEEE Intl. Geoscience and Remote Sensing Symp.* (pp. 2956-2958). Piscataway, NJ: IEEE. https://doi.org/10.1109/IGARSS.2003.1294644

Morton, C. G., Huntington, J. L., Pohll, G. M., Allen, R. G., McGwire, K. C., & Bassett, S. D. (2013). Assessing calibration uncertainty and automation for estimating evapotranspiration from agricultural areas using METRIC. *JAWRA, 49*(3), 549-562. https://doi.org/10.1111/jawr.12054

NDAWN. (2011). North Dakota Agricultural Weather Network Center. Fargo, ND: North Dakota State University. Retrieved from http://ndawn.ndsu.nodak.edu/

NDSWC. (2010). Devils Lake flood facts. Bismarck, ND: North Dakota State Water Commission. Retrieved from http://www.swc.state.nd.us/4dlink9/4dcgi/GetContentPDF/PB-194/DLFactSheetR.pdf

Rhoades, J. D., & Loveday, J. (1990). Salinity in irrigated agriculture. In B. A. Stewart, & D. R. Nielsen (Eds.), *Irrigation of agricultural crops* (pp. 1089-1142). Agronomy Monograph No. 30. Madison, WI: ASA.

Rijal, I., Jia, X., Zhang, X., Steele Dean, D., Scherer Thomas, F., & Akyuz, A. (2012). Effects of subsurface drainage on evapotranspiration for corn and soybean crops in southeastern North Dakota. *J. Irrig. Drain. Eng., 138*(12), 1060-1067. https://doi.org/10.1061/(ASCE)IR.1943-4774.0000508

Semmens, K. A., Anderson, M. C., Kustas, W. P., Gao, F., Alfieri, J. G., McKee, L., ... Velez, M. (2016). Monitoring daily evapotranspiration over two California vineyards using Landsat 8 in a multi-sensor data fusion approach. *Remote Sens. Environ., 185*, 155-170. http://dx.doi.org/10.1016/j.rse.2015.10.025

Sharma, V., Irmak, S., Kilic, A., & Mutiibwa, D. (2015). Application of remote sensing for quantifying and mapping surface energy fluxes in south central Nebraska: Analyses with respect to field measurements. *Trans. ASABE, 58*(5), 1265-1285. https://doi.org/10.13031/trans.58.11091

Singh, R. K., & Irmak, A. (2009). Estimation of crop coefficients using satellite remote sensing. *J. Irrig. Drain. Eng., 135*(5), 597-608. https://doi.org/10.1061/(ASCE)IR.1943-4774.0000052

Singh, R. K., Irmak, A., Irmak, S., & Martin, D. L. (2008). Application of SEBAL model for mapping evapotranspiration and estimating surface energy fluxes in south-central Nebraska. *J. Irrig. Drain. Eng., 134*(3), 273-285. https://doi.org/10.1061/(ASCE)0733-9437(2008)134:3(273)

SRP. (2017). SRP stores water for tomorrow. Phoenix, AZ: Salt River Project (SRP). Retrieved from https://www.srpnet.com/water/waterbanking.aspx

Steele, D. D., & Hopkins, D. G. (2010). Devils Lake basin water utilization test project. Final report. Fargo, ND: North Dakota State University.

Steele, D. D., Sajid, A. H., & Prunty, L. D. (1996). New corn evapotranspiration crop curves for southeastern North Dakota. *Trans. ASAE, 39*(3), 931-936. https://doi.org/10.13031/2013.27578

Steele, D. D., Thoreson, B. P., Hopkins, D. G., Clark, B. A., Tuscherer, S. R., & Gautam, R. (2015). Spatial mapping of evapotranspiration over Devils Lake basin with SEBAL: Application to flood mitigation via irrigation of agricultural crops. *Irrig. Sci., 33*(1), 15-29. https://doi.org/10.1007/s00271-014-0445-1

Stegman, E. C. (1982). Corn grain yield as influenced by timing of evapotranspiration deficits. *Irrig. Sci., 3*(2), 75-87. https://doi.org/10.1007/bf00264851

Stegman, E. C. (1986). Efficient irrigation timing methods for corn production. *Trans. ASAE, 29*(1), 203-210. https://doi.org/10.13031/2013.30127

Stegman, E. C. (1989). Soybean yields as influenced by timing of ET deficits. *Trans. ASAE, 32*(2), 551-557. https://doi.org/10.13031/2013.31038

Sumner, D. M. (1996). Evapotranspiration from successional vegetation in a deforested area of the Lake Wales Ridge, Florida. USGS Water Resources Investigations Report 96-4244. Reston, VA: U.S. Geological Survey.

Twine, T. E., Kustas, W. P., Norman, J. M., Cook, D. R., Houser, P. R., Meyers, T. P., ... Wesely, M. L. (2000). Correcting eddy-covariance flux underestimates over a grassland. *Agric. Forest Meteorol., 103*(3), 279-300. http://dx.doi.org/10.1016/S0168-1923(00)00123-4

UNW-AIS. (2013). Introduction to spate irrigation. Bonn, Germany: UN-Water Activity Information System. Retrieved from http://www.ais.unwater.org/ais/mod/page/view.php?id=215

USDA-NASS. (2007). 1:100,000-scale 2006 cropland data layer, a crop-specific digital data layer for North Dakota. Washington, DC: USDA National Agricultural Statistics Service.

USDA-NASS. (2008). 1:100,000-scale 2007 cropland data layer, a crop-specific digital data layer for North Dakota. Washington, DC: USDA National Agricultural Statistics Service.

USDA-NASS. (2009). 1:100,000-scale 2008 cropland data layer, a crop-specific digital data layer for North Dakota. Washington, DC: USDA National Agricultural Statistics Service.

USDA-NRCS. (2011). Soil Survey Geographic (SSURGO) database for Towner County, North Dakota. Washington, DC: USDA Natural Resources Conservation Service. Retrieved from http://soildatamart.nrcs.usda.gov

USDA-SCS. (1982). North Dakota irrigation guide. IG Notice ND-4. Washington, DC: USDA, Soil Conservation Service.

USGS. (2011). EarthExplorer. Reston, VA: U.S. Geological Survey. Retrieved from https://earthexplorer.usgs.gov/

USGS. (2012). 2001 National Land Cover Data (NLCD 2001). Sioux Falls, SD: USGS Earth Resources Observation and Science (EROS Center, Multi-Resolution Land Characteristics Consortium. Retrieved from https://www.mrlc.gov/nlcd2001.php

Wang, K., & Dickinson, R. E. (2012). A review of global terrestrial evapotranspiration: Observation, modeling, climatology, and climatic variability. *Rev. Geophys., 50*(2), article RG2005. https://doi.org/10.1029/2011RG000373

Wilson, K., Goldstein, A., Falge, E., Aubinet, M., Baldocchi, D., Berbigier, P., ... Verma, S. (2002). Energy balance closure at FLUXNET sites. *Agric. Forest Meteorol., 113*(1-4), 223-243. https://doi.org/10.1016/S0168-1923(02)00109-0